N92-14366

DYNAMIC CHARACTERISTICS AND STABILITY ANALYSIS OF SPACE SHUTTLE MAIN ENGINE OXYGEN PUMP

Edgar J. Gunter and Lyle Branagan
Department of Mechanical and Aerospace Engineering
University of Virginia
Charlottesville, Virginia 22903, U.S.A.

This paper deals with the dynamic characteristics of the Space Shuttle high pressure oxygen pump. Experimental data is presented to show the vibration spectrum and response under actual engine operation and also in spin pit testing for balancing. The oxygen pump appears to be operating near a second critical speed and is sensitive to self excited aerodynamic cross coupling forces in the turbine and pump. An analysis is presented to show the improvement in pump stability by the application of turbulent flow seals, preburner seals, and pump shaft cross sectional modifications.

INTRODUCTION

This paper deals with the dynamic characteristics and stability analysis of the oxygen pump employed in the NASA Space Shuttle Main Engine System. Both the hydrogen and oxygen pumps for the SSME are supported on rolling element bearings. These bearings have little inherent damping. As a result of low bearing damping, self excited whirl motion was observed on the hydrogen pump in early tests. Investigations conducted on stability at the University of Virginia and also by D. Childs at Texas A&M, indicated that turbulent flow seals could substantially increase the stability characteristics of the hydrogen pumps. The theory of turbulent flow seals as originally developed by Black, and expanded upon by Allaire and Childs, was applied to the oxygen pump preburner end. A substantial improvement in rotor stability of the oxygen pump could be achieved by stiffening the cross section of the preburner shaft section.

PUMP DESCRIPTION

The oxygen pump consists of a double suction main impeller driven by two stages of overhung turbine. The oxygen pump weighs 77 lbs. and is designed to operate at 29,000 RPM (FPL). The design power of the oxygen pump is approximately 31,000 horsepower.

Figure 1 represents a schematic cross-section of the SSME rocket engine. The oxygen pump, labeled HPOTP, for high pressure oxygen turbopump, appears on one side of the figure. On the opposite side of the figure is the high pressure fuel turbopump, which supplies liquid hydrogen to the rocket nozzle. The liquid oxygen and hydrogen, supplied to the nozzles, are fed in to the combustion chamber of the rocket engine. There are three rocket engines on each shuttle craft. The high pressure oxygen turbopump is designed to supply LOX (liquid oxygen) at 1,153 lbs. per second to the engine.

The supply pressure to the main pump is 4,974 psi and the supply pressure to the small preburner pump is 8,070 psi.
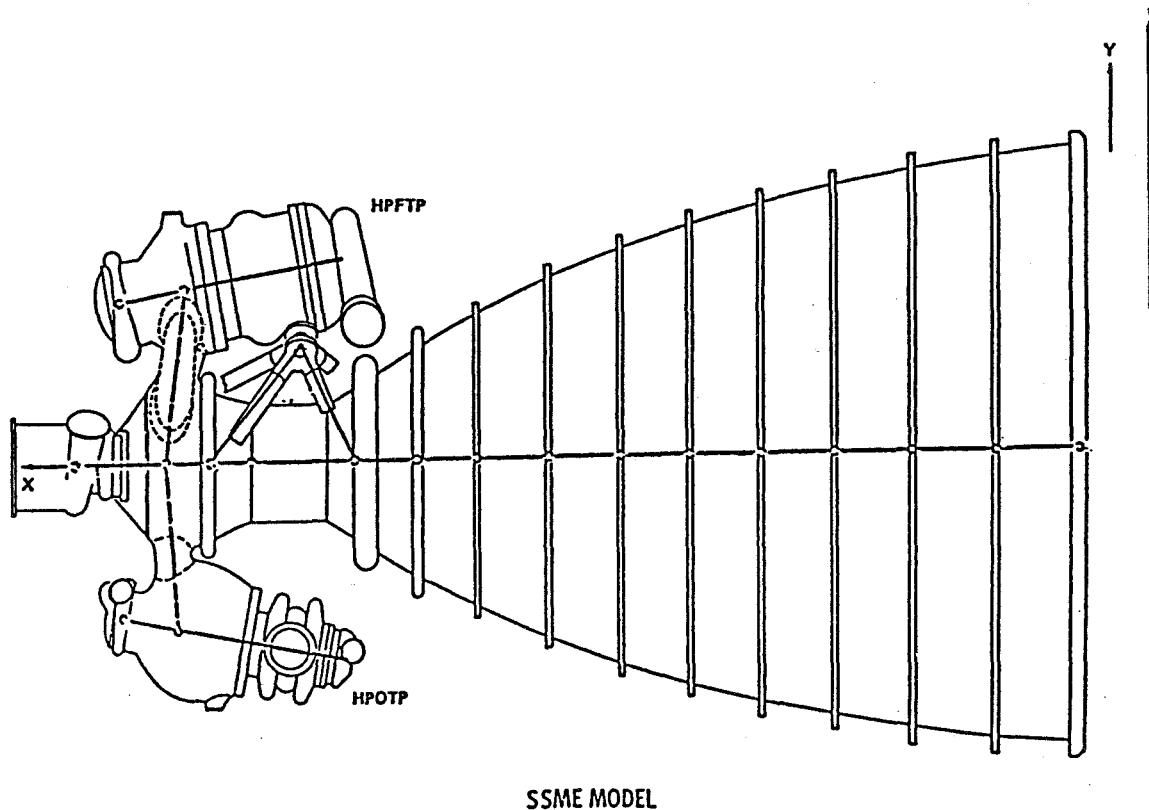

FIGURE 1 SPACE SHUTTLE MAIN ENGINE (SSME) MODEL

Figure 2 represents the cross-section of the HPOTP rotor. The rotor is supported at the pump-end (left) by two 45 mm ball bearings and at the turbine-end (right) by two 55 mm ball bearings. At the right, is shown the two-stage, hot-gas turbine, which drives the oxygen pump. The main pump is represented by the central impeller and is of a dual flow configuration. The impeller wheels act as a balance piston for this design. In a conventional turbopump, a mechanical axial thrust bearing, absent in both the oxygen and hydrogen pumps, takes up the axial load. Overhung from the pump bearing and attached to the main shaft is the preburner impeller. The preburner impeller is used to provide oxygen for the combustion which powers the turbine stages. The oxygen rotor is designed such that it must be assembled. The main impeller slides onto the turbine section and is held in place with a lock nut. The preburner impeller is assembled after the preburner bearings have been positioned.
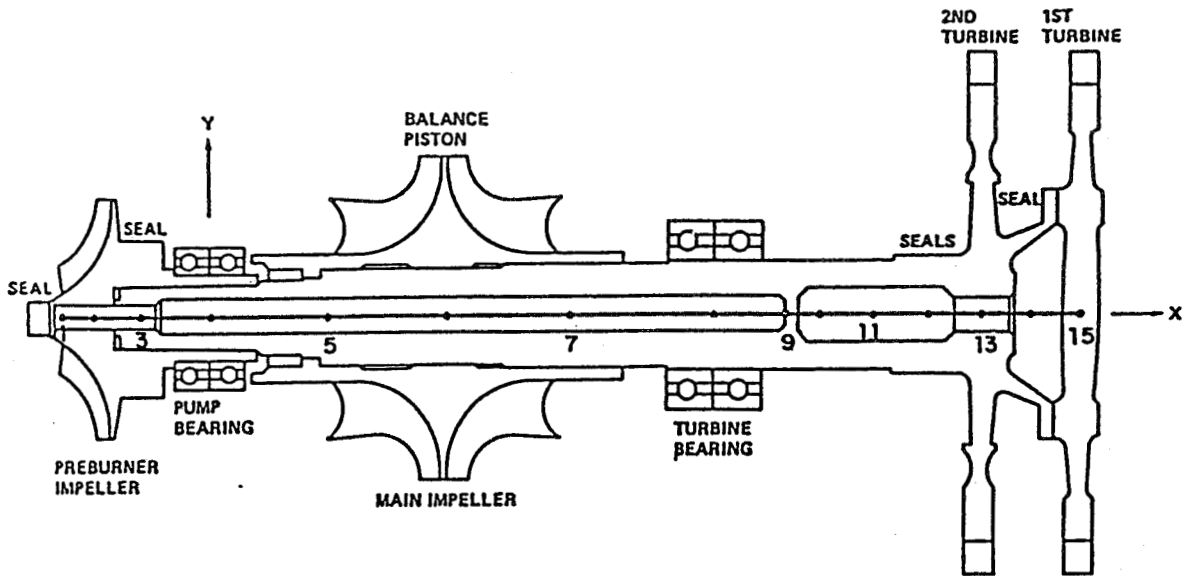
HPOTP ROTOR MODEL

FIGURE 2   HIGH PRESSURE OXYGEN TURBOPUMP (HPOTP) ROTOR MODEL

Figure 3 represents the HPOTP case model.   The HPOTP case model shows the location of the impellers, turbine, bearings, and various seals in the pump.
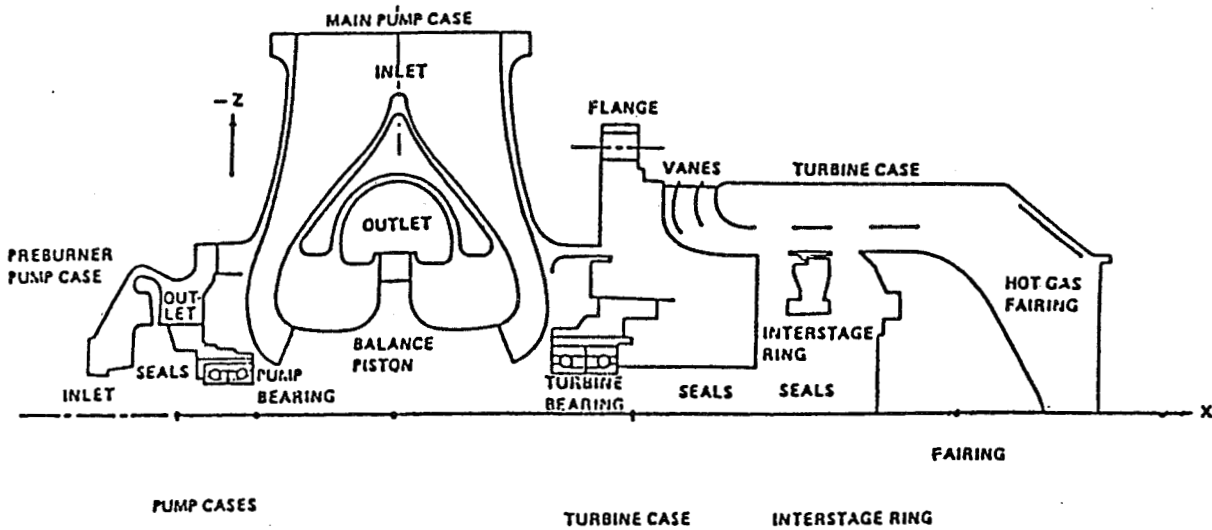
HPOTP CASE MODEL

MODEL "A" (Original NASA Model)

FIGURE 3   HIGH PRESSURE OXYGEN TURBOPUMP (HPOTP) CASE MODEL

319

The oxygen pump was designed to operate from 22,000 RPM (MPL - minimum power level) to 29,000 RPM (FPL - full power level) and is to be free of critical speeds in this vicinity. The design time of operation of the oxygen pump during FPL is approximately 730 seconds.

REVIEW OF EXPERIMENTAL DATA

Figure 4 represents the experimental data obtained during NASA test run 902-065. This figure shows the synchronous motion of a radial accelerometer as a function of oxygen pump shaft speed for both runup and rundown. On runup, two major resonant peaks are clearly seen: approximately, 22,000 RPM and 27,000 RPM. Upon rundown a very predominant peak at 26,000 RPM is observed. According to the original design specifications, there should not be any critical speeds in the operating speed range.
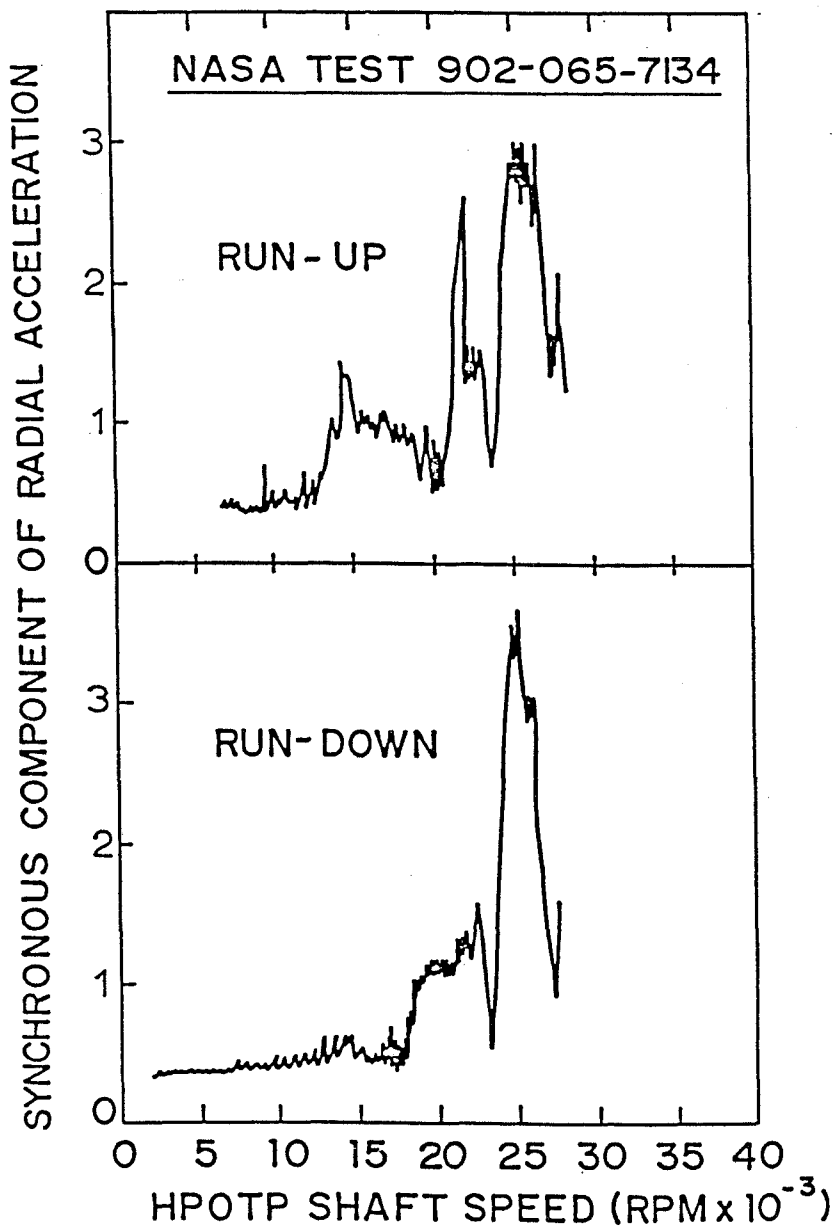

FIGURE 4   HPOT RADIAL 45° ACCELEROMETER

Figure 5 represents the same NASA test run (902 - 065), but in this case, the synchronous motion of the oxygen pump casing accelerometer was tracked as a function of hydrogen shaft speed. Since the hydrogen pump operates at a slightly higher speed, the hydrogen pump acts as a vibration exciter, and the synchronous tracking filter (synchronous with the hydrogen pump speed) produces an indication of which resonant frequencies are within this operating speed range.
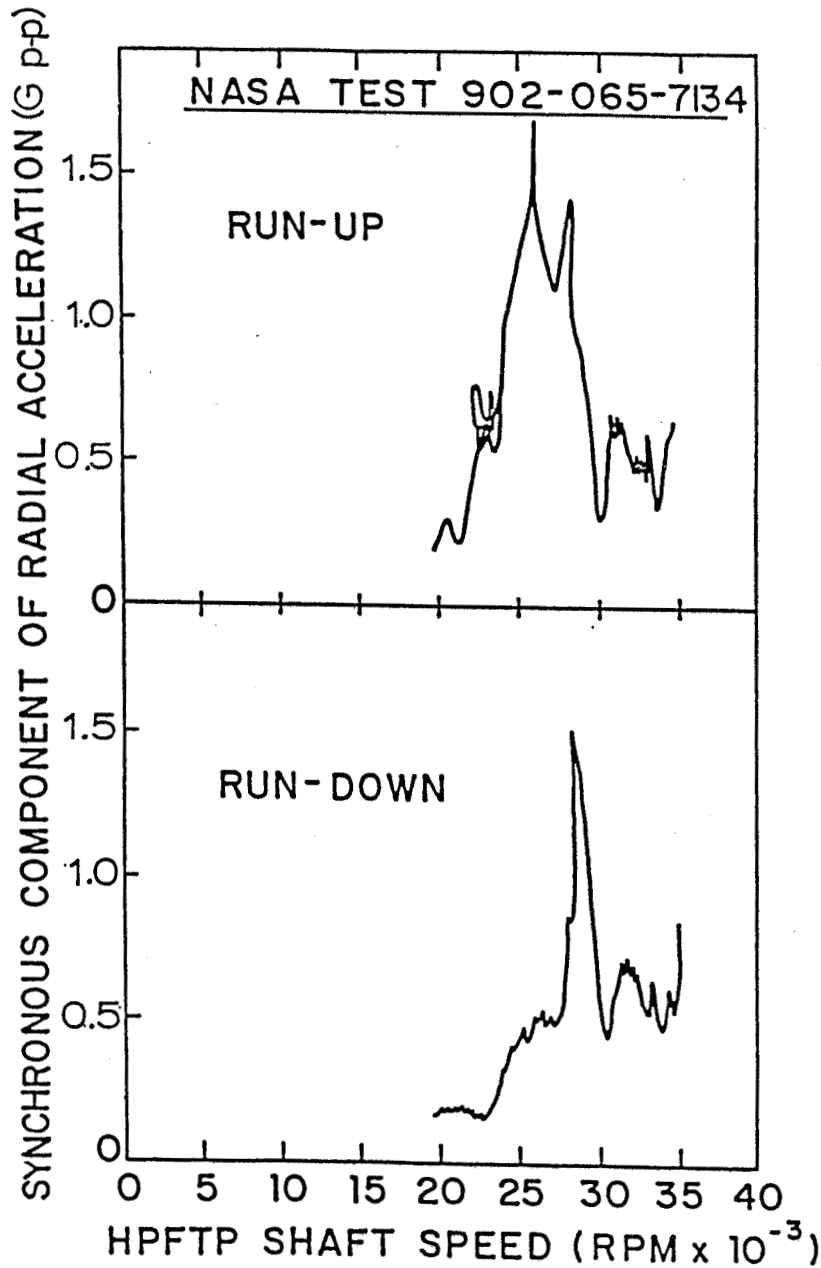

FIGURE 5 HPOT RADIAL 45° ACCELEROMETER

From the curve on runup, it is seen that there is a resonant frequency at approximately 25,000 RPM. This information corresponds with the vibration data obtained on runup and rundown as a function of hydrogen or oxygen pump speed. Also observed is a resonant frequency at approximately 28,000 RPM. Upon rundown, this is the predominant frequency observed. From this data, it therefore appears that there are three distinct resonant frequencies in the operating speed range. These resonant frequencies are approximately 22,000 RPM, 26,000 RPM, and 28,000 RPM. The 540 degree phase shift indicates the passage through these three resonant frequencies (Figure 6).
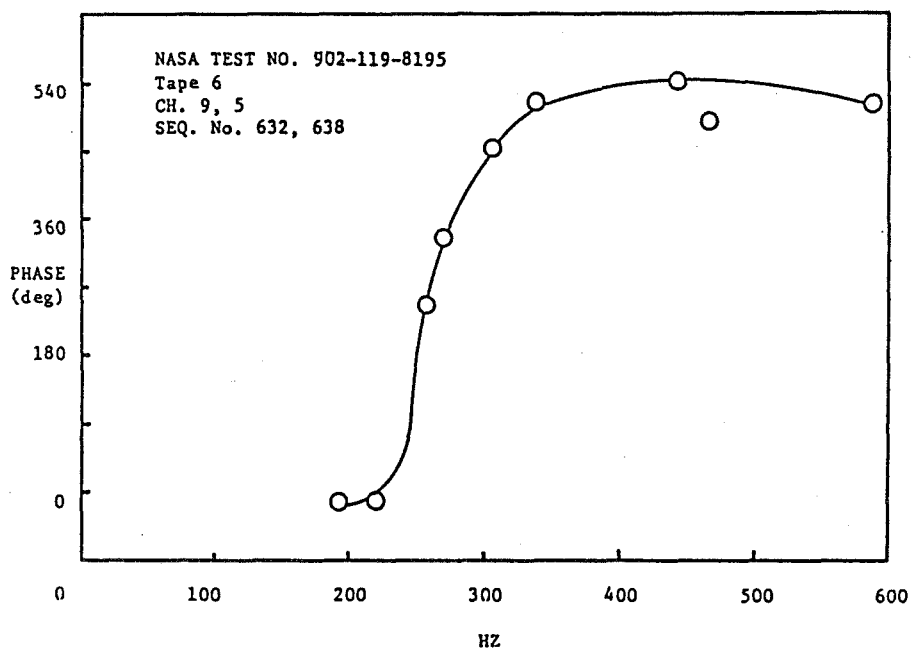

FIGURE 6 PHASE ANGLE BETWEEN HPOT RADIAL 135° AND PBP RADIAL
135° ACCELEROMETERS

Figure 7 represents the frequency spectrum obtained on NASA run 902-119 for the preburner axial 90° accelerometer for speeds ranging from 60% RPL to 100% RPL. In this figure, one is able to discern a low level oxygen pump motion which may be associated with the whirl of the oxygen pump at the first critical speed. This dotted line is designated "O_2 whirl." The frequency spectrum also shows the amplitude due to oxygen pump speed and to hydrogen pump speed. The frequency spectrum shows that there is an oxygen pump resonant frequency at approximately 378 Hz and at 466 Hz (which corresponds to 100% RPL). The amplitude increase indicates a possible resonant speed. The hydrogen pump speed is also clearly seen on this figure with peaks at 468 Hz, and at 587 Hz (the operating speed of the hydrogen pump). It appears that the hydrogen pump may also be operating on a resonant frequency. The fact that the hydrogen pump speed peaks at 468 Hz also indicates a possible oxygen pump resonant frequency at the hydrogen pump operating speed.
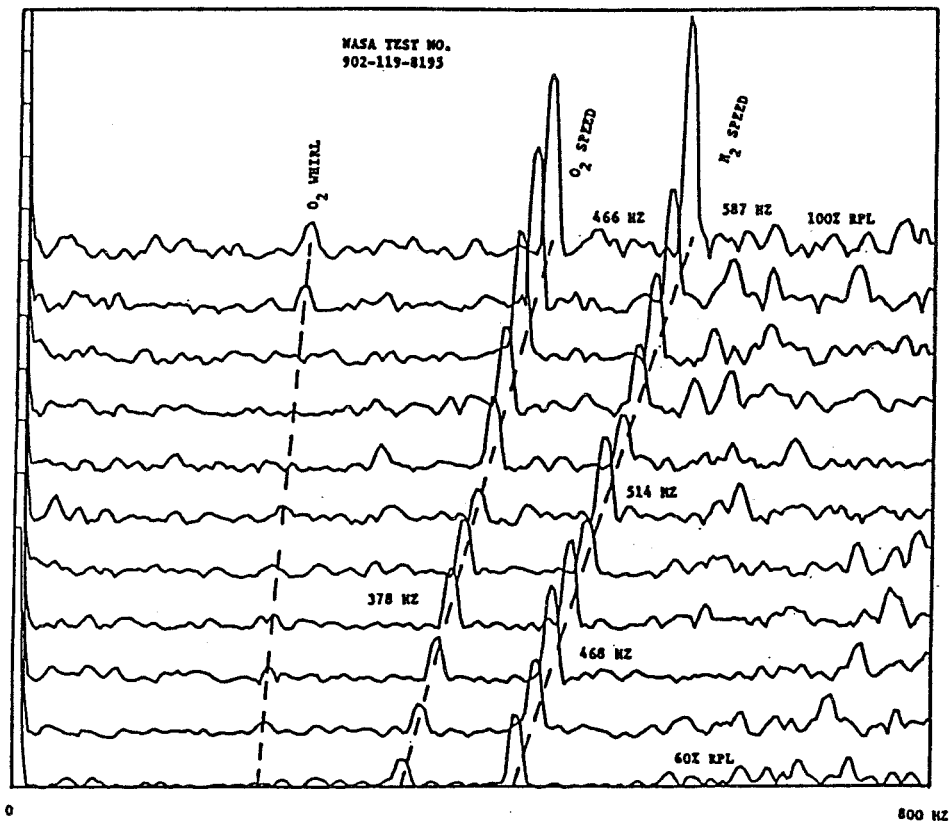
FIGURE 7   PBP AXIAL 90° ACCELEROMETER CASCADE DIAGRAM

Figure 8 represents the synchronous radial acceleration of the oxygen rotor as a function of oxygen pump shaft speed (NASA test 910-136). During runup, two resonances were observed at 22,000 and 25,500 RPM. The resonance at 25,500 RPM appears to dominate. This speed corresponds to operation at 90% rated power level. Upon reaching rated power level, the speed was reduced and the rotor was operated at 90% RPL. Due to continued operation at this speed, the rotor amplitude increased until failure occurred. The upper figure represents the phase angle change while passing through the 25,000 RPM speed range. The 180 degree phase shift shown corresponds to passage through a resonant frequency.

Run 902-193 was a later run of the S.S.M.E. in which the system was operated to 109% of the rated power level. Several spectrums of this run are shown to illustrate the response frequencies encountered with the oxygen and hydrogen pumps.

Figure 9 represents the peak hold spectrum from 0 to 500 Hz encountered with the HPOP 45 degree radial accelerometer. This figure shows that a frequency of 232 Hz at a level of 4 Grms was encountered during acceleration from 0 to 100% RPL. The value of 232 Hz could correspond to the oxygen pump first critical speed. This frequency, in general, was not very pronounced during deceleration.

Figure 10 represents the peak channel hold accelerometer spectrum of the HPOP 45° radial accelerometer during deceleration from 109% to 90 RPL. Not that there is a pronounced resonant frequency at 463 Hz. The magnitude of the peak amplitude is 10 Grms.

323
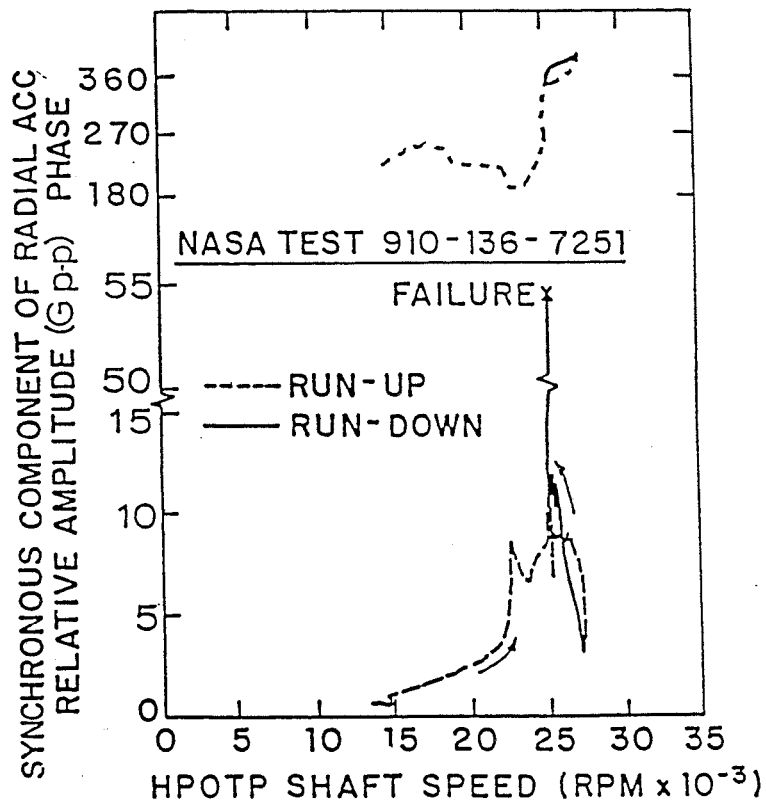
FIGURE 8 SYNCHRONOUS ACCELERATION FOR HPOP RADIAL
ACCELEROMETER DURING FAILURE RUN
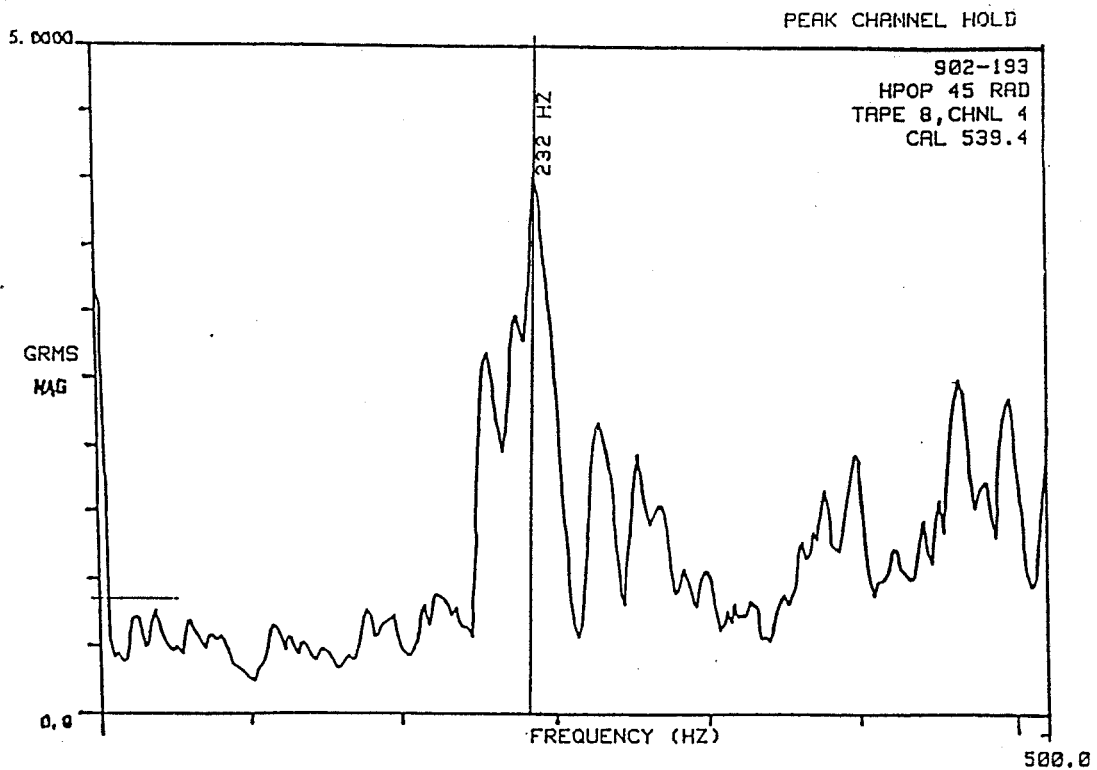
FIGURE 9 HPOP - ENGINE ACCELERATION (0-100% RPL)

324
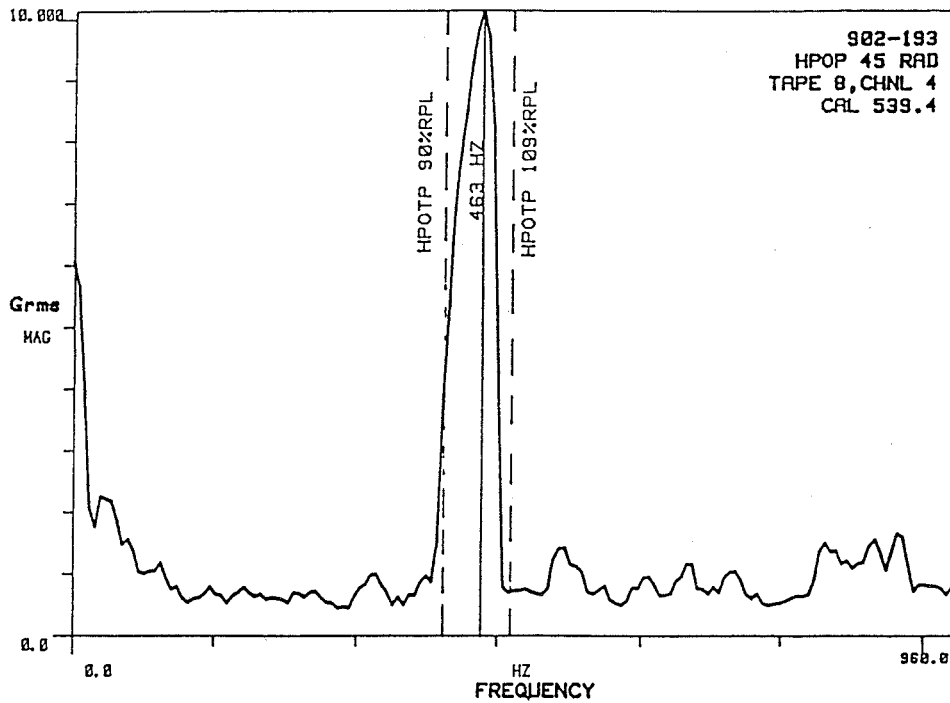
FIGURE 10 HPOP - ENGINE DECELERATION (109-90% RPL)

Examination of the various other accelerometers on the oxygen pump showed a similar characteristic. For example, Figure 11 represents the peak channel hold spectrum for the HPOT 90° accelerometer during the entire coast down from 109% to 0% RPL. Note that this accelerometer shows a peak resonant frequency at 453 Hz.

FIGURE 11 HPOT - ENGINE COASTDOWN (109-0% RPL)

325

The data of Run 902-193 indicates that the oxygen pump has a major resonant frequency between 450 and 470 Hz. This response frequency could represent the second critical speed of the oxygen pump. This mode may be particularly sensitive to excitation, because a nozzle bending mode is also predicted in this range.

SCOPE OF INVESTIGATION

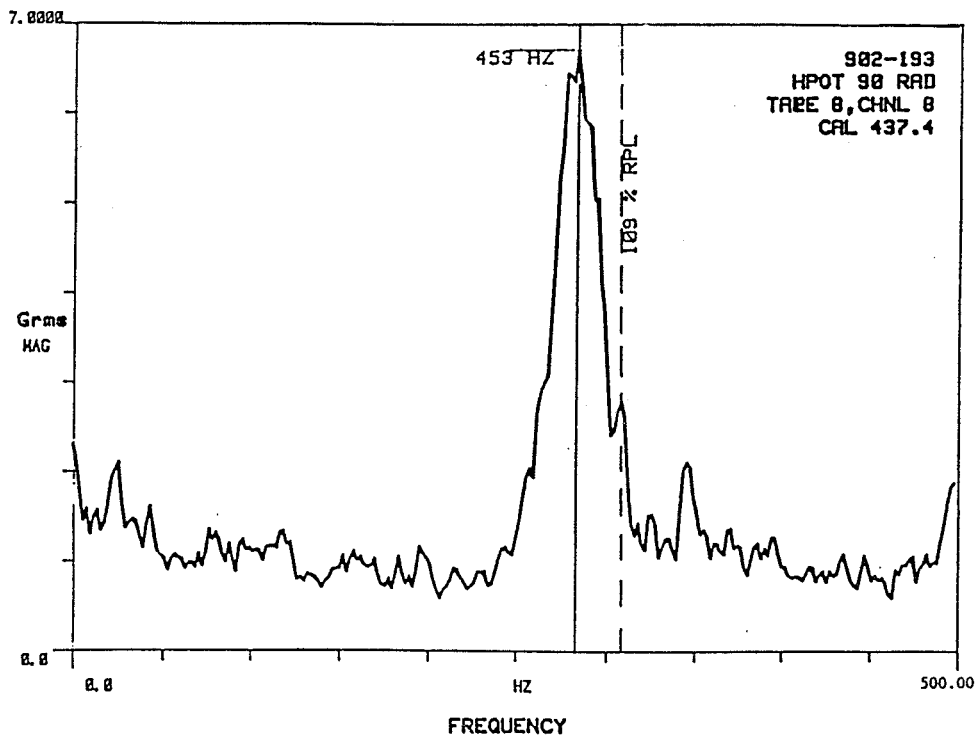One of the major considerations for the stability analysis of the high pressure oxygen pump is the influence of cross-coupling generated by the turbine stages, the main impeller, and the seals. The major seal locations are at the preburner impeller, at the turbine bearing and between turbine stages. The main areas where aerodynamic cross-coupling may be generated are the main impeller and turbine stations.

The critical speeds and stability characteristics for the oxygen pump are highly dependent upon the values of bearing stiffness and damping assumed for the various bearing and seal location. The values for ball bearing stiffness used are modified from experimental data. The values for seal stiffness and damping used were taken from Childs' report. Additional seal and shaft modification were also considered in order to evaluate their influence on stability.

In the experimental analysis of the Space Shuttle Main Engine System, it has been observed that the hydrogen shaft speed is recorded on the oxygen pump accelerometers. The transfer of motion, from one system to another, is due in part to the flexibility and dynamic characteristics of the engine nozzle and hot gas manifold. In this analysis, however, the flexibility of the hydrogen pump, nozzle, and oxygen pump casings are not included.

It is therefore the objective of this investigation to identify the critical speeds and stability characteristics of the oxygen pump only as a function of bearing and seal characteristics. The investigation concentrates on the effects of the bearing characteristics on the critical speeds to determine if an oxygen pump second critical speed could exist in the 460 Hz vicinity and if the pump should exhibit indications of instability.

CRITICAL SPEED ANALYSIS OF THE OXYGEN PUMP

Background

In the original design of the oxygen pump, it was assumed that there would be no critical speed in the operating speed range between MPL (minimum power level) and FPL (full power level). The only critical speed that the pump would incur, would be the first critical speed at approximately 16,000 RPM. Figure 12 represents the original oxygen pump critical speed map, assuming no seals and a rigid casing. Three critical speeds are shown in this field map. Superimposed on the critical speed map are the effective bearing stiffnesses, originally assumed to be present in the oxygen pump for two different ranges of bearing clearance: 1.37 mils and 2.63 mils. The first critical speed was estimated to be 14,000 RPM and the second critical speed was estimated to be 38,000 RPM. A value of 38,000 RPM would place the oxygen pump second critical speed well above the maximum operating speed of the oxygen pump.

One of the earliest indications that the actual stiffnesses may not be as high as previously predicted was obtained from experimental information generated while attempting to balance the pump. Figure 13 represents the oxygen pump rotor unbalance response (4.76 gm-in unbalance located at the preburner location) while being balanced in the spin pit facility. To more clearly indicate the resonant frequency present in the system, the data was conditioned by subtracting the low speed runout for Run

326

13 of the No. 2 Bently Probe. As can be seen from the amplitude-versus-speed curves experimentally obtained, there is a first critical speed at 10,000 RPM and a second critical speed at 25,600 RPM. The second critical speed obtained in the experimental spin test facility corresponds closely with the incident run of NASA test 910-136.
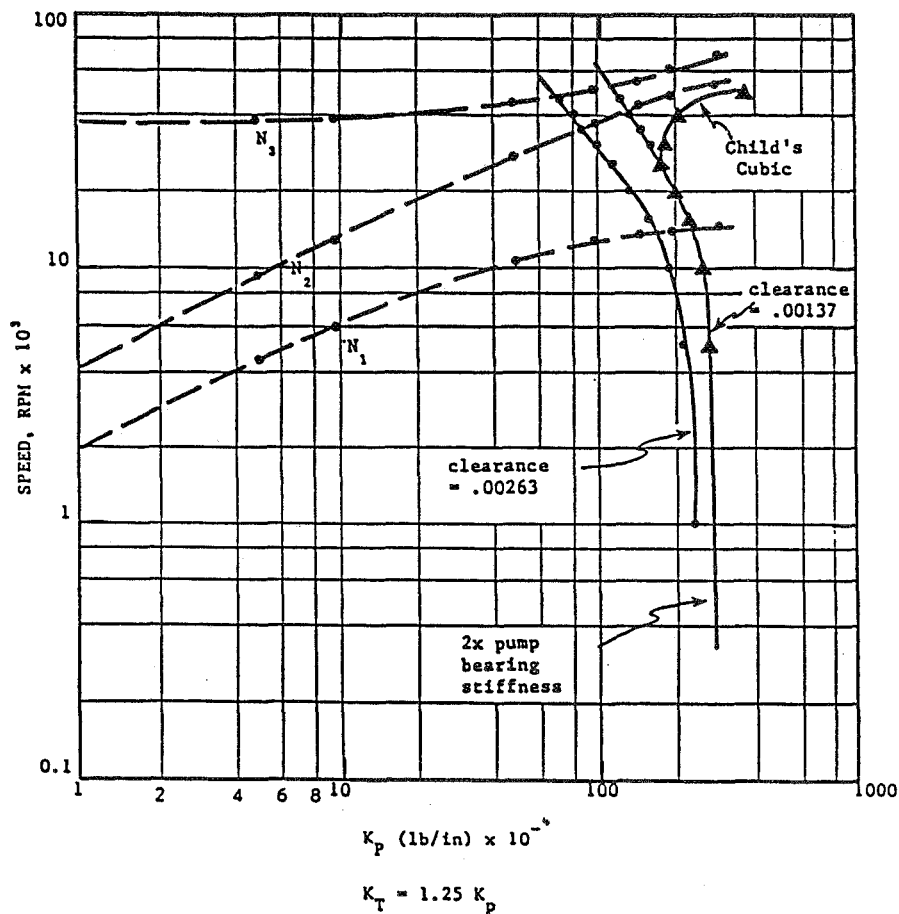

FIGURE 12 ORIGINAL OXYGEN PUMP CRITICAL SPEED MAP - NO SEALS AND RIGID CASING

In the balance test run on the oxygen pump, it was observed that unbalance at the preburner location had very little effect on the turbine end location and also little response at the first critical speed. An unbalance at the turbine end had a large response at 10,000 RPM, but a little response at the second critical speed of 25,600 RPM. Thus, the experimental spin pit data indicates that the second mode is predominantly a preburner and main impeller mode with little motion at the turbine end. Therefore, if this second mode were excited in the oxygen pump at rated speeds, one would expect to see large amplitudes of motion at the main impeller and preburner locations. Close examination of the failed oxygen pump from run 910-136 indicated possible contacting at either the preburner or main impeller; the turbine end was relatively undamaged. Figure 13 also indicates that after passage through the second critical speed the amplitude, a minimum of 28,000 RPM, begins to increase rapidly again, indicating the onset of a third critical speed.
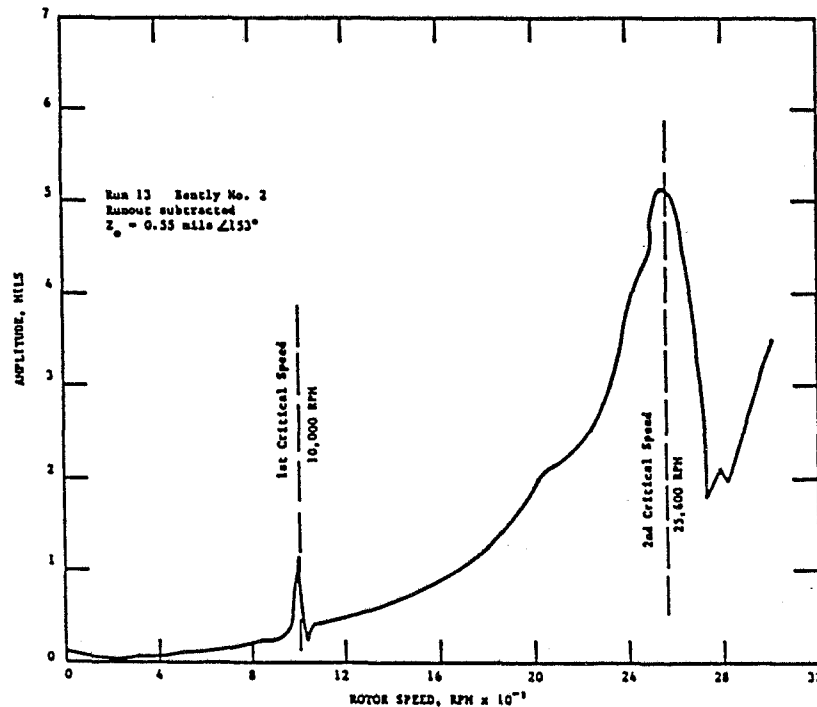
FIGURE 13 OXYGEN PUMP ROTOR UNBALANCE RESPONSE WITH 4.76 GM-IN
AT PREBURNER LOCATION - RUNOUT SUBTRACTED

In order to obtain critical speeds of 10,000 and 25,600 RPM, the original critical speed map indicates that the combined stiffness of the preburner bearings is only 400,000 lb/in, and the combined stiffness of the turbine bearings is only 500,000 lb/in, rather than 1,200,000 lb/in, as originally predicted for the turbine bearings.

Data obtained from the balance spin pit facility on low speed phase and amplitude runout was not repeatable with small unbalance at the preburner end. Such data may indicate that the shaft joints of the preburner and main impeller shift around with unbalance when driven to the second critical speed. This may account for the difficulty encountered in attempting multiplane balancing of the oxygen pump over the two critical speeds.

Computer Models

Critical speeds and mode shapes have been calculated by Rocketdyne, NASA, and the University of Virginia. A lumped mass-elastic section model of the rotor derived from computer analysis was provided to the University by NASA. This model consists of 15 shaft sections with areas, lengths, and inertia properties; shaft diameters were derived from the inertia terms. A second model (UVA) was created using a scale drawing of the pump cross-section. Diameters, taken from the drawing, were combined with the weights, lengths, and inertia terms of the NASA model. Figure 14 shows the three cross sections superimposed on one another. Although the actual rotor has hollow cross sections, both computer models use a solid shaft approximation.

328

CROSS-SECTIONS

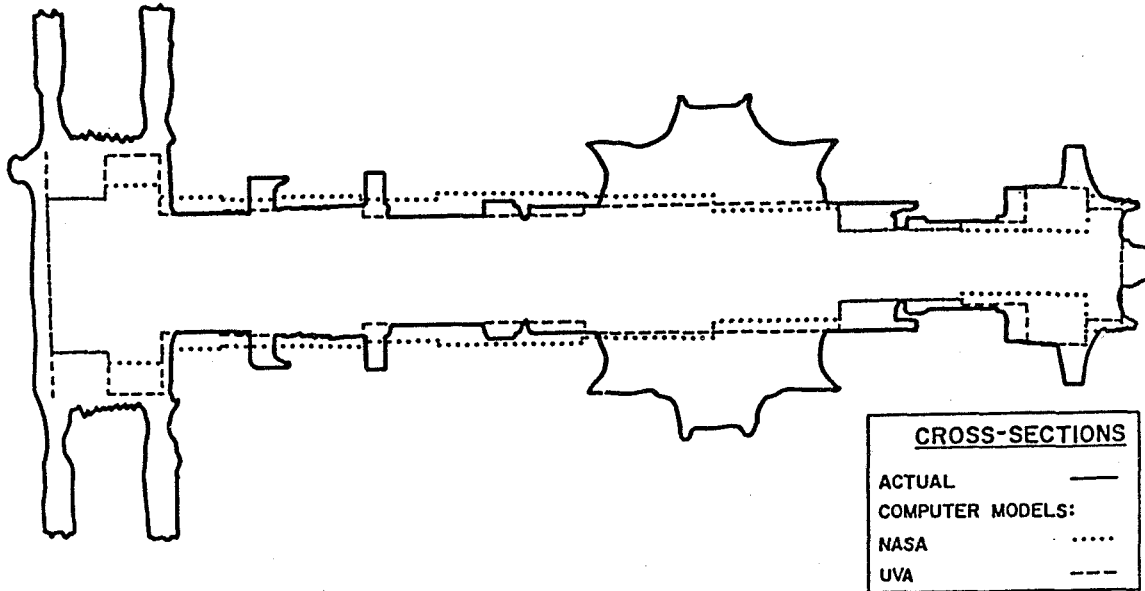ACTUAL   —
COMPUTER MODELS:
NASA   ·····
UVA   ———

FIGURE 14

There is considerable difference between NASA model and the UVA model at the preburner bearing at the turbine locations. For example, the NASA model assumes a thinner section at the preburner bearing than is assumed by the UVA model. This would accentuate the bending problems of the oxygen pump at the second critical speed. Also, the NASA model assumes a thicker section at the turbine shaft location (station 10) than actually exists (See Table 1). Although one may use experimental data on which to base a computer model, it is not justified to assume a cross section which is thicker than the actual model. Therefore, additional modifications of the NASA model could be done to improve its accuracy.

TABLE 1   COMPARISON OF COMPUTER MODELS FOR OXYGEN PUMP
ROTOR

ROTOR MODEL: NASA   ROTOR MODEL: UVA

STATION NUMBER	LENGTH (IN)	OUTSIDE DIAMETER (IN)	WEIGHT (LB)	STATION NUMBER	LENGTH (IN)	OUTSIDE DIAMETER (IN)	WEIGHT (LB)
1	0.772	2.800	0.669	1	0.772	2.3	0.669
2	1.070	1.340	2.377	2	1.070	3.2	2.378
3	1.558	1.347	3.042	3	1.558	1.7	3.043
4	2.583	1.518	1.290	4	2.583	1.5	1.290
5	2.640	2.270	7.757	5	2.640	2.6	7.757
6	2.640	2.975	13.392	6	2.640	2.6	13.392
7	3.170	3.105	8.607	7	3.170	2.2	8.606
8	1.560	2.931	3.404	8	1.560	2.2	3.403
9	0.800	3.102	4.197	9	0.800	2.7	4.197
10	1.120	3.102	0.101	10	1.120	2.6	0.101
11	1.200	3.050	2.473	11	1.200	2.5	2.473
12	1.170	3.102	1.877	12	1.170	2.4	1.877
13	1.115	3.742	12.514	13	1.115	5.0	12.514
14	1.117	3.090	3.415	14	1.117	3.1	3.416
15	0.0	3.090	13.825	15	0.0	5.0	13.825

Critical Speed Analysis

Although there are considerable differences between the UVA and the NASA models, their predictions for the occurrence of the second critical speed are almost identical. Figure 15 represents the oxygen pump first and second forward critical speeds assuming an operating speed of 27,000 RPM. Using the revised combined preburner bearing stiffness of 476,000 lb/in from turbine bearing (Ref. Childs), the first critical speed predicted by the UVA model is 11,000 RPM and the first critical speed predicted by the NASA model is 13,000 RPM. Both models predict the second critical speed at approximately 27,000 RPM.

OXYGEN PUMP
UNDAMPED FORWARD CRITICAL
SPEED MAP
N = 27,000 RPM
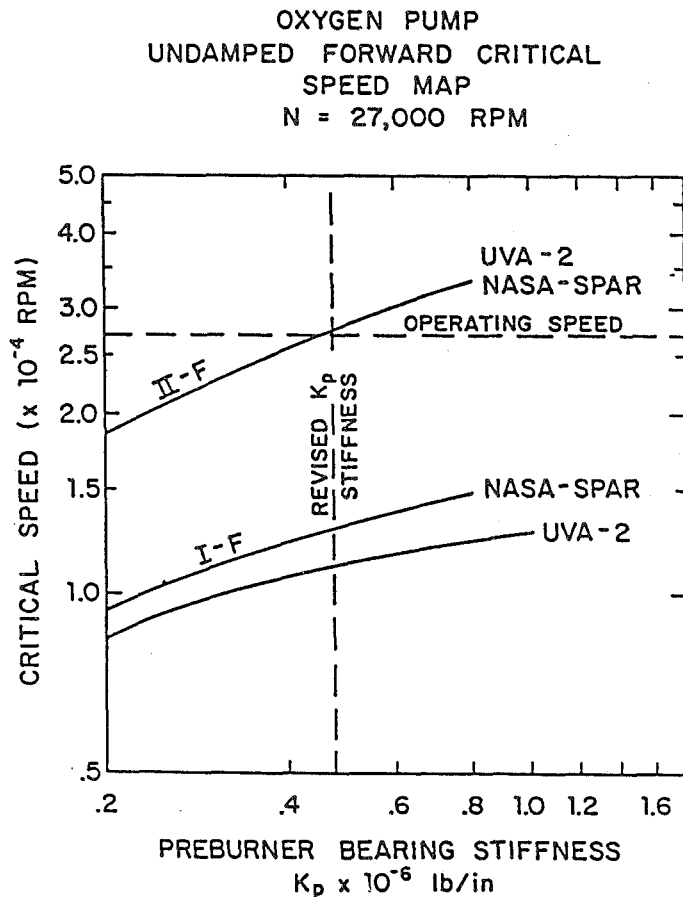
FIGURE 15

As an additional check on the critical speed calculations, a computer program to calculate the forward and backward critical speeds (CRITSPD) was developed by Dr. Gunter. In this particular case, undamped seals as well as bearings were considered. Assuming that the oxygen pump is operating at 27,000 RPM, the forward critical speeds were predicted to be 13,000 RPM, 26,858 RPM and 37,569 RPM.

Another reason for developing the new critical speed program was to calculate the strain energy distribution between the shaft and bearings. Table 2 represents the oxygen pump critical speed and percent of total strain energy in the shaft and the bearings. For example, the table shows that in the first mode 25% of the total strain energy is in rotor bending and 75% is in the bearings. It is of

330

interest to note that the preburner bearing only carries 3% of the strain energy for the first mode; the majority of the energy from shaft bending occurs near the turbine bearing location. One could assume therefore that the preburner bearing stiffness has little influence on the location of the first critical speed. The preburner and the turbine ends of the shaft have little strain energy. Therefore, the first critical speed is predominantly affected by the main turbine bearing and interstage turbine seal.

TABLE 2   CRITICAL SPEED SUMMARY
Critical Speed Analysis of SSME Oxygen Pump
at 27,000 RPM with Derated Bearings

Forward Whirl Analysis

NO. MODE	CRITICAL SPEED (RPM)	SHAFT (% of total	BEARING strain energy)
1	13,000	25	75
2	26,858	19	81
3	37,569	52	48

STATION NO.	FIRST CRITICAL SPEED SHAFT (% of strain energy)	BEARING	SECOND CRITICAL SPEED SHAFT (% of strain energy)	BEARING	THIRD CRITICAL SPEED SHAFT (% of strain energy)	BEARING
1	0		0		0	
2	0	0	0	2	0	13
3	0		0		0	
4	0	3	0	50	5	28
5	1		7		31	
6	1		5		5	
7	3		5		5	
8	13	34	3	29	5	7
9	6		0		1	
10	1		0		0	
11	0		0		0	
12	0	9	0	0	0	0
13	0		0		0	
14	0	29	0	0	0	0
15	0		0		0	

[Note: seal strain energy is included under BEARING]

At the second critical speed, predicted to be 26,858 RPM, 81% of the strain energy is in the bearings and 19% is in the shaft. Half of the system strain energy is in the preburner bearing and only 29% is in the main turbine bearing. It is important to note that there is little strain energy connected with either the preburner or the turbine shaft locations. The major strain energy of the shaft is associated with sections 4 through 7, which are the preburner bearing and main impeller locations. From the strain energy distribution of the second mode, it is apparent why the NASA model and the UVA model match in predicting of the second critical speed; this is because the second critical speed is being controlled predominantly by the preburner bearing stiffness. The thickness of the turbine end location has negligible effect on the second critical speed.

A third critical speed of 37,569 RPM is predicted. In this mode, the strain energy is divided equally between the shaft and the bearings. However, at this third mode, the major part of the bearing strain energy is carried at the preburner seal and at the preburner bearing. The fact that over 30% of the total strain energy occurs in only one shaft section, station 5, indicates a considerable amount of local bending.

The experimental data in Figure 7 indicates that the hydrogen pump amplitude appears to increase with speed. If the hydrogen pump has a high level of amplitude at 37,000 RPM, it may excite the oxygen pump third critical speed. It is apparent that this frequency can be increased only by stiffening up the shaft section at this location. The occurrence of the critical speed of the oxygen pump at 37,000 RPM may explain why the experimental data in the experimental test rig (Figure 13) shows amplitude beginning to increase rapidly above 28,000 RPM; the oxygen pump may have been approaching its third critical speed, essentially an overhung preburner mode.

Figure 16 represents the oxygen pump forward and backward critical speeds for various operating rotor speeds, assuming the derated bearing stiffness characteristics. Due to the gyroscopics of the overhung disk, main impeller and preburner ends; forward and backward critical speeds appear. For example, at 27,000 RPM, the difference between first forward and backward critical speeds is 4,000 RPM. The second backward critical speed is approximately 24,325 RPM and the second forward is 26,879 RPM, a difference of 2,500 RPM. The difference between forward and backward critical speeds increase with operating speed. These values of forward and backward critical speeds were calculated using the program ROTSTB, and they correspond closely with the predicted forward and backward values obtained from the CRTSPD program.
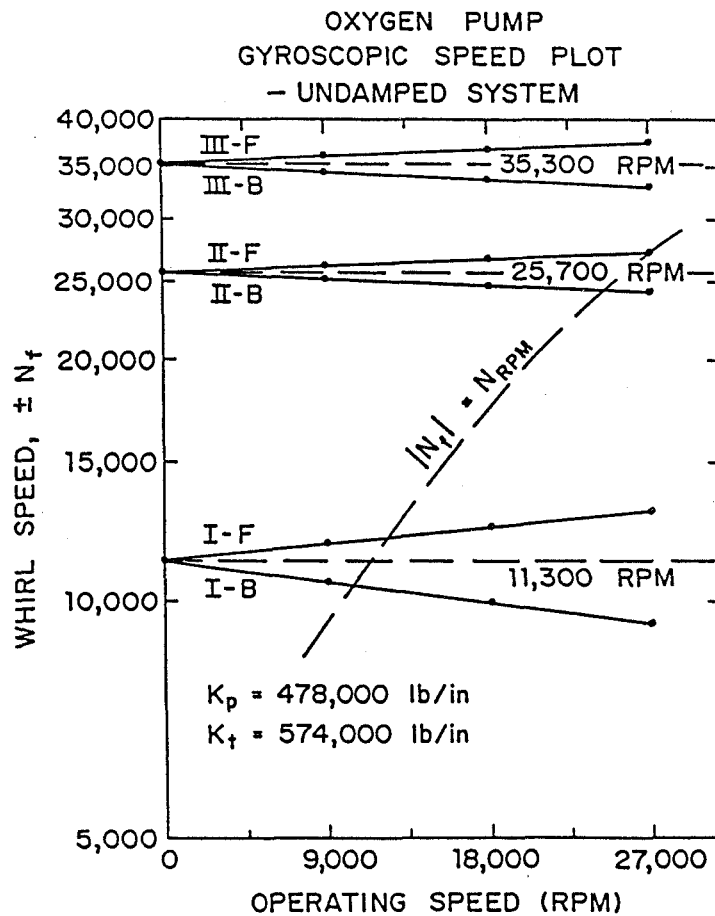

OXYGEN PUMP
GYROSCOPIC SPEED PLOT
— UNDAMPED SYSTEM

FIGURE 16

332

Normally, the occurrence of backward critical speeds in a turborotor is of little concern, since unbalance in a turborotor will excite only the critical speeds of forward synchronous precession. In the case of the SSME configuration, however, in which the oxygen pump is cantilevered off the main nozzle, excitation from the hydrogen pump and nozzle may be transmitted to the oxygen casing by the hot gas manifold. Under these circumstances, a planar excitation could conceivably excite a backward as well as a forward mode. Observation of the experimental data, Figures 4 and 5, shows weak modes at approximately 22,000 and 33,000 RPM. It may be possible that these modes are backward excitations of the oxygen pump.

Figure 17 represents first forward undamped critical speed for the oxygen pump operating at 27,000 RPM. Reduced bearing stiffnesses of 400,000 lb/in for the preburner bearing and 600,000 lb/in for the turbine bearing were assumed. Using the ROTSTB stability program, the first forward critical speed was predicted to be 10,661 RPM. This value correlates well with the critical speeds predicted by Rocketdyne, but is somewhat lower than the value calculated using CRTSPD which includes the effect of seals. It also corresponds well with the critical speeds observed in the spin pit, in which seals were not present. As can be seen from the first mode shape, the maximum amplitude occurs at the overhung turbine and rapidly diminishes as one approaches the preburner end. At a distance of 12 inches from the preburner end, the amplitude is a node point. The small preburner motion is out of phase with the motion of the turbine end.
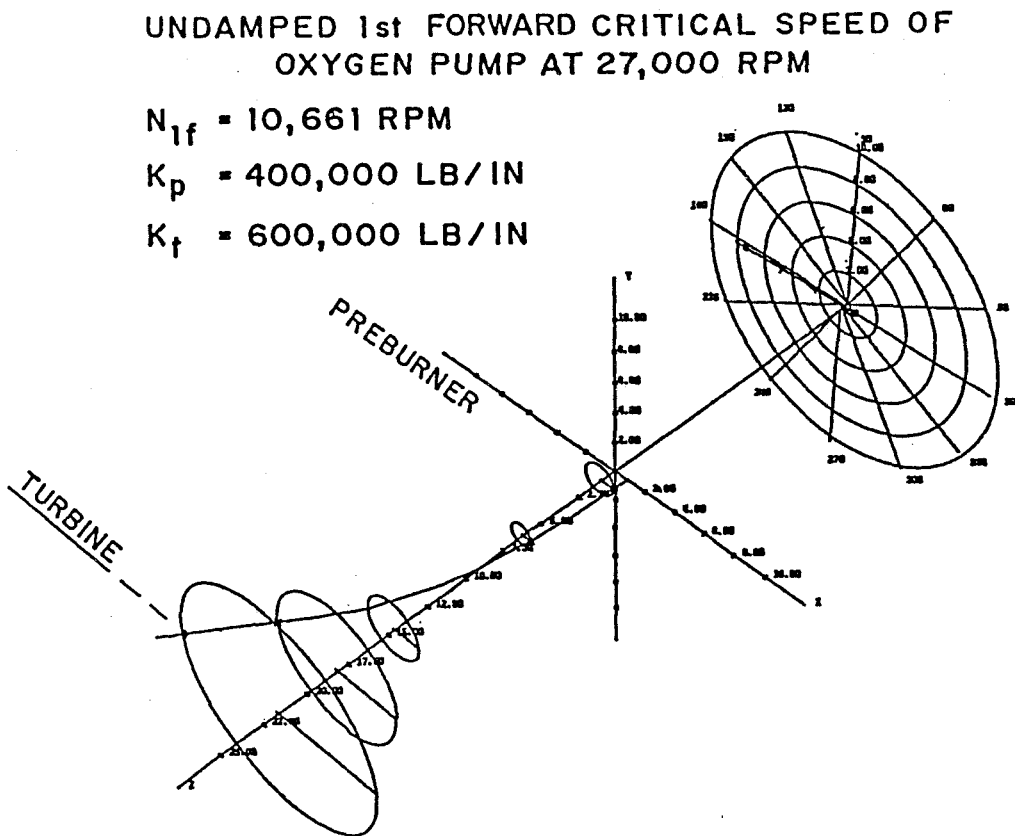

UNDAMPED 1st FORWARD CRITICAL SPEED OF
OXYGEN PUMP AT 27,000 RPM

N_{1f} = 10,661 RPM

K_p = 400,000 LB/IN

K_t = 600,000 LB/IN

FIGURE 17

333

The mode shape, as depicted in Figure 18 for the second forward critical speed without seals, shows that the second critical speed occurs at 25,350 RPM. Examination of the 3-dimensional mode shape, reveals that the turbine motion is a node point and that the maximum amplitude occurs at the main and preburner impellers. It is readily apparent that any attempts to improve the rotor response at 27,000 RPM by trim balancing the turbine stages will have little beneficial effect; balancing must be done at the preburner or main impeller location.

In the undamped critical speed plots, depicted by Figures 17 and 18, the mode shapes were made nondimensional. In an actual rotor, the response of the rotor at a particular speed will be a function of the unbalance distribution and the damping in the system. These figures imply that the rotor cannot be successfully balanced through both critical speeds by single plane balancing of the turbine stage. If the second critical speed cannot be successfully balanced at the preburner impeller due to spline slippage, then the oxygen pump should be redesigned.

UNDAMPED 2nd FORWARD CRITICAL SPEED OF OXYGEN PUMP AT 27,000 RPM

$N_{2f} = 25,350$ RPM

$K_p = 400,000$ LB/IN

$K_t = 600,000$ LB/IN
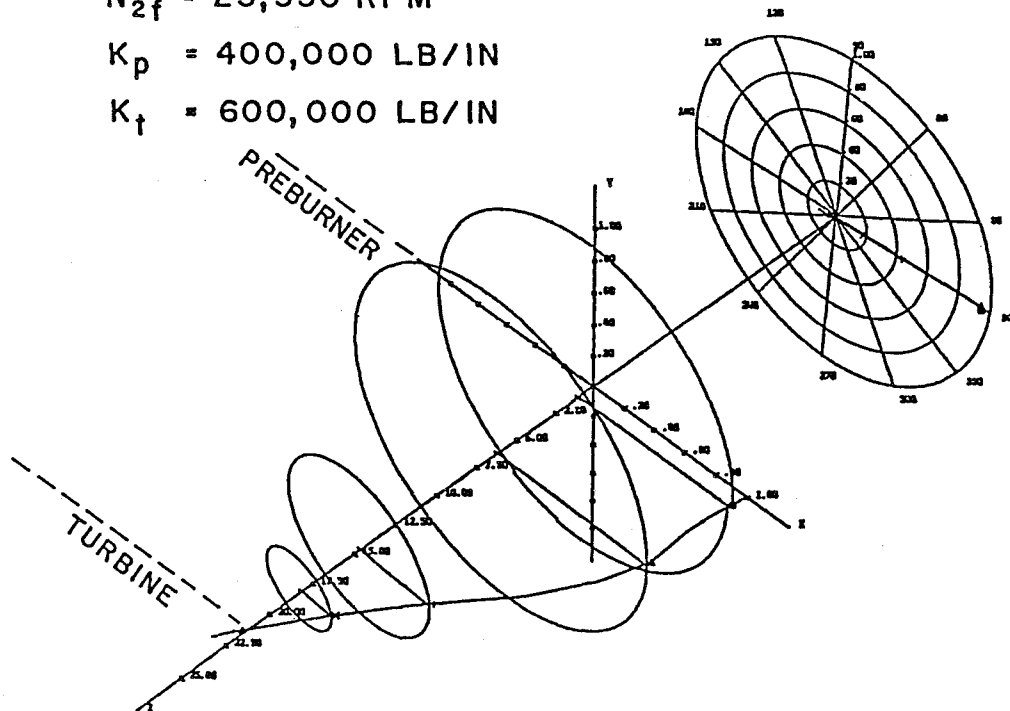
FIGURE 18

STABILITY ANALYSIS: DAMPED MODES

In considering the stability of the oxygen pump rotor, the effects of seal aerodynamic cross-coupling, as well as bearing and seal damping, were investigated. Stiffness and damping characteristics for each of the six seals were taken from a report by D. Childs and were lumped together at three seal locations: preburner seals, turbine seals, and turbine interstage seals. The bearings were modeled using

the derated stiffnesses and minimal damping. The overall stiffness and damping matrix used in the initial stability analysis is presented in Table 3. Aerodynamic effects were later added by means of cross-coupling terms acting at the midpoint of the main impeller. The UVA rotor model was used for the stability analysis because of its better agreement with the experimental critical speed data. The NASA model, with its stiffer turbine section would tend to exaggerate the stability of the first bending mode, an overhung turbine mode.

TABLE 3   STIFFNESS AND DAMPING MATRIX CHILD'S VALUES

(DAMPING AND CROSS-COUPLING)

STATION NUMBER	STIFFNESS				
	K_{xx} (LB/IN)	K_{yx} (LB/IN)	K_{xy} (LB/IN)	K_{yy} (LB/IN)	
2	30,000	-17,000	17,000	30,000	PREBURNER SEAL
4	476,000	0	0	476,000	PREBURNER BEARING
8	574,000	0	0	574,000	TURBINE BEARING
12	21,210	- 4,560	4,560	21,210	TURBINE SEAL
14	38,630	-26,000	26,000	38,360	INTERSTAGE (TURBINE) SEAL

DAMPING

	C_{xx} (LB-SEC/IN)	C_{yx} (LB-SEC/IN)	C_{xy} (LB-SEC/IN)	C_{yy} (LB-SEC/IN)
2	10.5	0.	0.	10.5
4	2.0	0.	0.	2.0
8	2.0	0.	0.	2.0
12	2.8	0.	0.	2.8
14	14.0	0.	0.	14.0

Undamped conditions used a nominal 5.0 lb-sec/in at each station.

Stability calculations, using the rotor stability program ROTSTB, indicate that both bending modes encountered in the operation of the oxygen pump are unstable. Figure 19 displays the sources of this instability. Cross-coupling forces generated by the interstage and turbine tip seals (26,000 lb/in) are forty percent in excess of the theoretical cross-coupling required to destabilize the first mode. While a cross-coupling of 10,450 lb/in acting on the main impeller is sufficient for instability of the second mode, initial calculations indicate that aerodynamic forces could generate aerodynamic cross coupling of the order of 30,000 to 40,000 lb/in. The analysis further indicates that the two modes are independent and that modification must consider both modes.
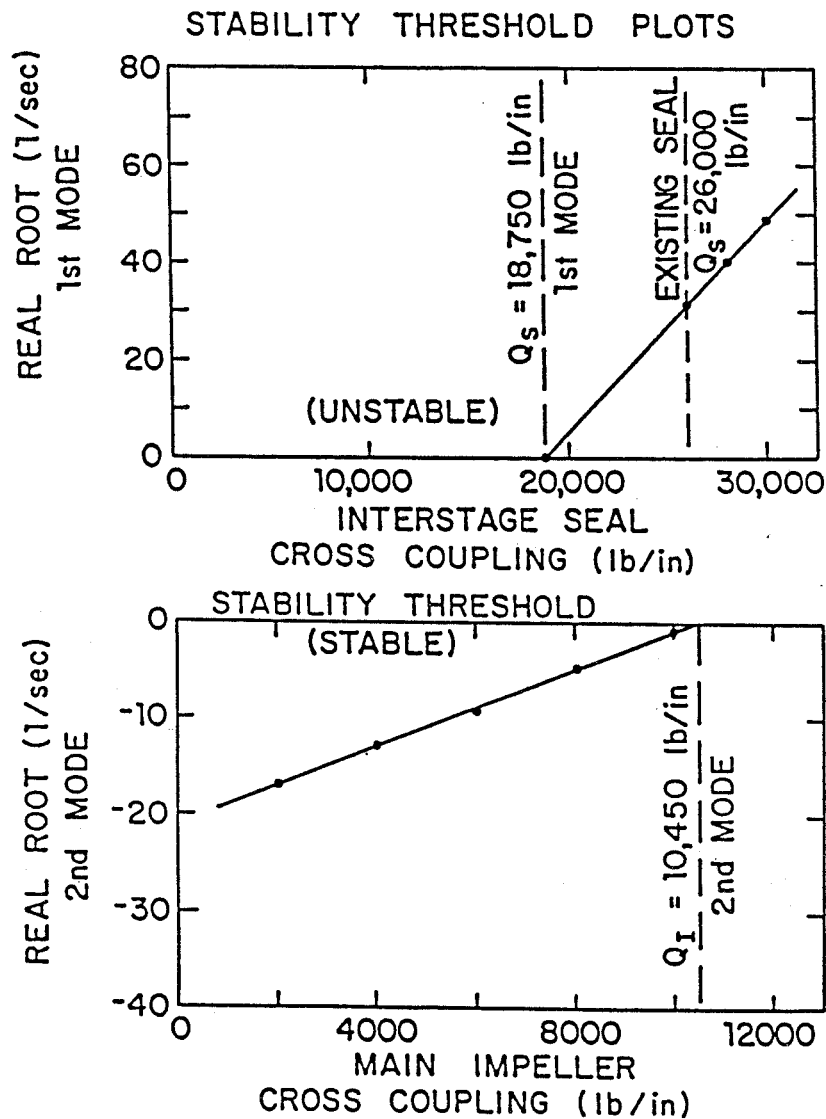
STABILITY THRESHOLD PLOTS

FIGURE 19

The stability analysis in this report assumes a smooth seal acting at the turbine interstage location. D. Childs also presented the stiffness and damping characteristics for the labyrinth seal originally included in the oxygen pump design. Stability calculations with the UVA model, derated bearings, and full seals, substituting the labyrinth interstage seal for the smooth seal, indicate that the rotor is unstable. The configuration with the labyrinth seal, however, is closer to the threshold of stability than with the smooth seal. Further, the first critical frequency is lowered slightly, although there is little effect on the second or third critical frequencies. This indicates that the original labyrinth seal design should be more stable than the smooth configuration.

The most promising modification to improve stability appears to be combining a stiffer turbine bearing with a softer pump bearing and with additional damping at the preburner seals. Varied independently, none of these factors have an appreciable influence on the stability of this system. Varying the damping coefficients and the turbine bearing stiffness at the same time seems to produce the most marked improvement. These results are shown in Figure 20. With the pump bearing stiffness damping exponent of the first mode; however, the effect is asymptotic. A modification of the shaft geometry seems required.

336

1st MODE OXYGEN PUMP STABILITY FOR VARIOUS VALUES OF PREBURNER SEAL DAMPING C_p vs. TURBINE BEARING STIFFNESS K_t

Figure showing ROOT P (1/sec) 1st MODE vs. TURBINE BEARING STIFFNESS $K_t \times 10^{-6}$ (lb/in). Curves labeled $C_p = 10.5$, $C_p = 50$, $C_p = 100$, $C_p = 200$ (solid, ORIGINAL ROTOR) and a dashed line $C_p = 10.5$ (STIFFENED ROTOR). $K_p = 476,000$ lb/in. Region marked (UNSTABLE).

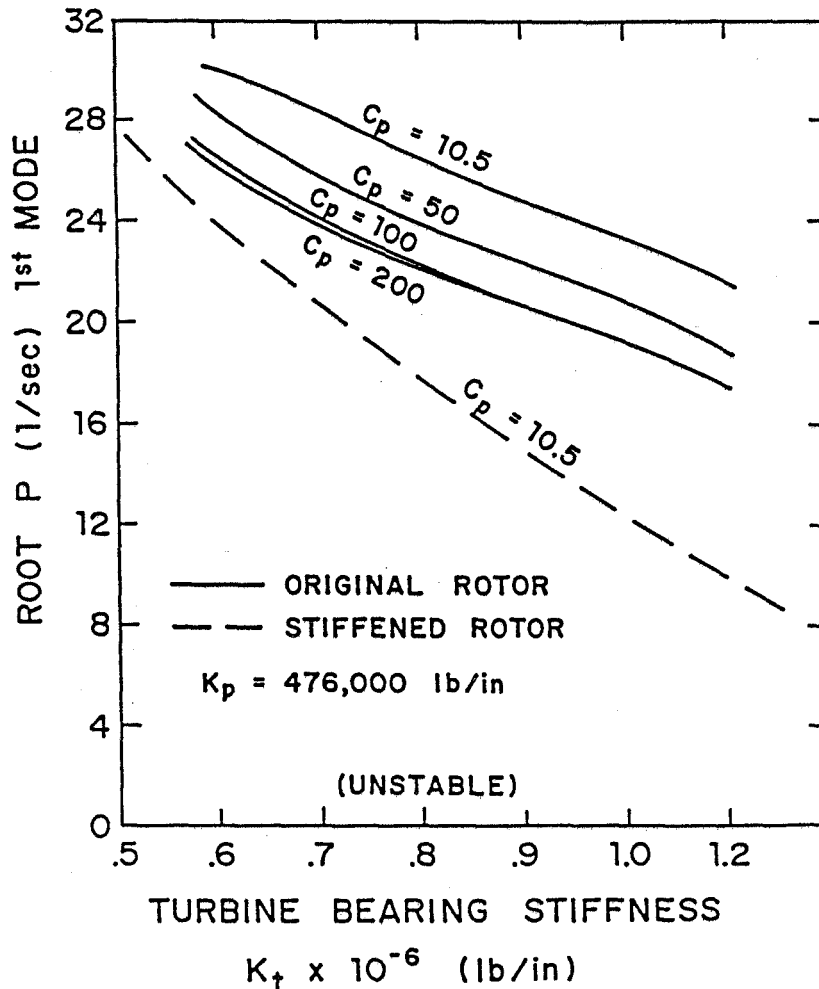TURBINE BEARING STIFFNESS
$K_t \times 10^{-6}$ (lb/in)

FIGURE 20

A third rotor model was created with a minimum shaft diameter of 2.6 inches at the bearings. The properties of this model, called "stiffened rotor," are presented in Table 4. Figure 21 presents the three rotor cross-sections used in this paper (with a compressed horizontal scale). The NASA model has thick turbine end sections and thin preburner end sections. The UVA model, which gave better agreement with the experimental critical speed data, has thin sections around the bearing locations. Finally, the stiffened rotor shows a nearly uniform cross-section from the preburner to the turbine stages. The dashed line, on Figure 21, portrays the stabilizing influence of this thicker cross section. While the stiffer rotor is an improvement, modification of the seals and bearings is also indicated.

337

TABLE 4 ROTOR MODEL: STIFFENED ROTOR

Section Data

STATION NUMBER	LENGTH (IN)	OUTSIDE DIAMETER (IN)	WEIGHT (LB)
1	0.772	2.3	0.669
2	1.070	3.2	2.378
3	1.558	2.6	3.043
4	2.583	2.6	1.291
5	2.640	2.6	7.757
6	2.640	2.6	13.392
7	3.170	2.6	8.607
8	1.560	2.6	3.403
9	0.800	2.7	4.197
10	1.120	2.6	0.101
11	1.200	2.6	2.473
12	1.170	2.6	1.877
13	1.115	5.0	12.514
14	1.117	3.1	3.416
15	0.0	5.0	13.825

ROTOR CROSS-SECTION MODELS FOR OXYGEN PUMP

NASA-SPAR

UVA2

STIFFENED ROTOR

ADDED SHAFT DIAMETER
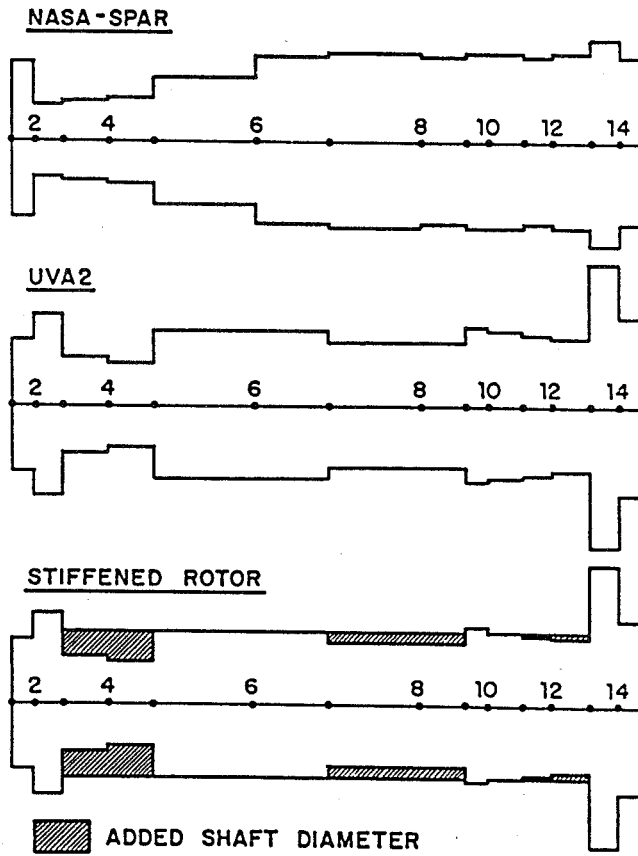
NOTE: HORIZONTAL SCALE IS ONE HALF VERTICAL SCALE.

FIGURE 21

338

The increase in rotor cross-section at the bearing locations implies bearing redesign. Figure 22 shows that with a significantly stiffer turbine bearing (1,200,000 lb/in) the stability of the first mode can be obtained with a wide choice of pump bearing stiffness and preburner seal damping coefficients.

The second mode presents two difficulties for the operation of the oxygen pump. Its critical frequency lies in the operating range of the pump, at approximately 100% RPL and it is unstable due to the aerodynamic forces on the main impeller. To observe the variation in the second forward critical speed as a function of the various parameters thus far considered, Figure 23 was prepared. This figure corresponds with Figure 22 and shows that a preburner bearing stiffness between 200,000 and 400,000 lb/in, along with the stiffened rotor, would be unacceptable for use in the oxygen pump operating speed range. Operation at a lower stiffness value would require a softer turbine bearing.
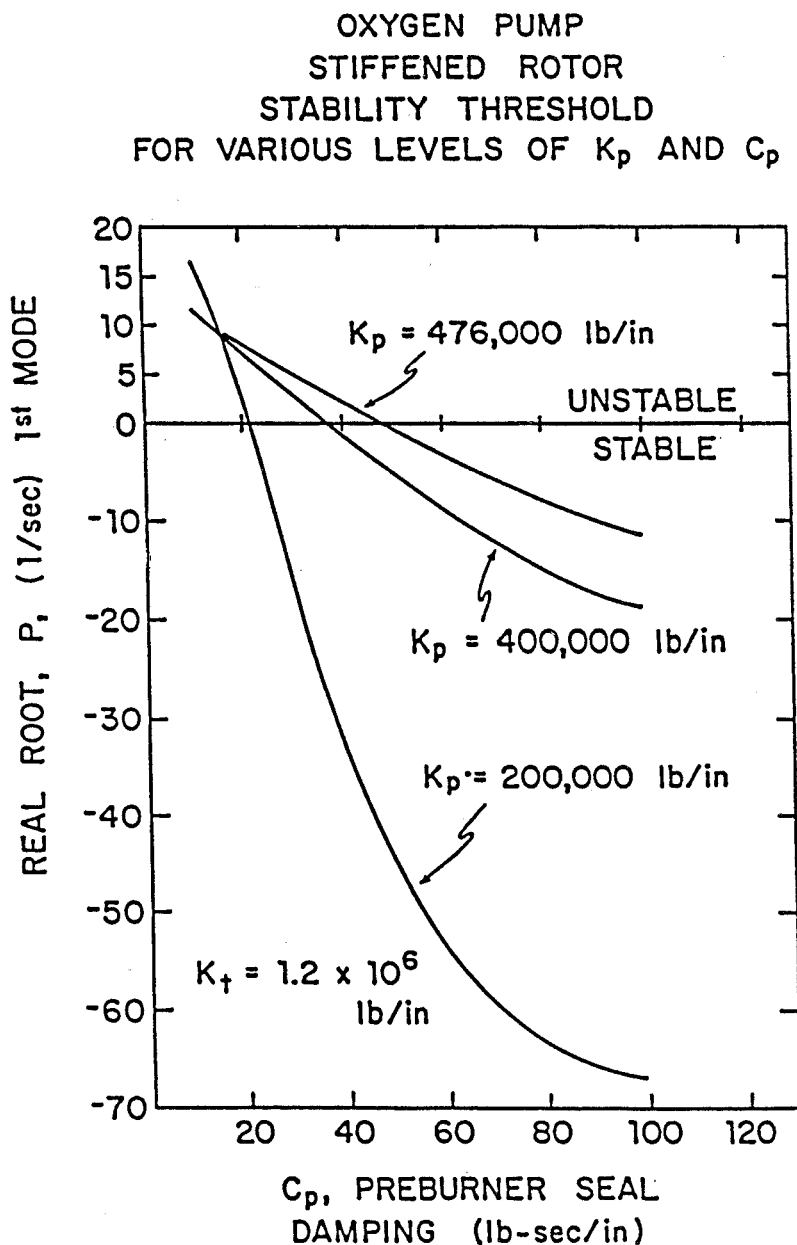
OXYGEN PUMP
STIFFENED ROTOR
STABILITY THRESHOLD
FOR VARIOUS LEVELS OF K_p AND C_p

FIGURE 22

OXYGEN PUMP
STIFFENED ROTOR
SECOND CRITICAL SPEED
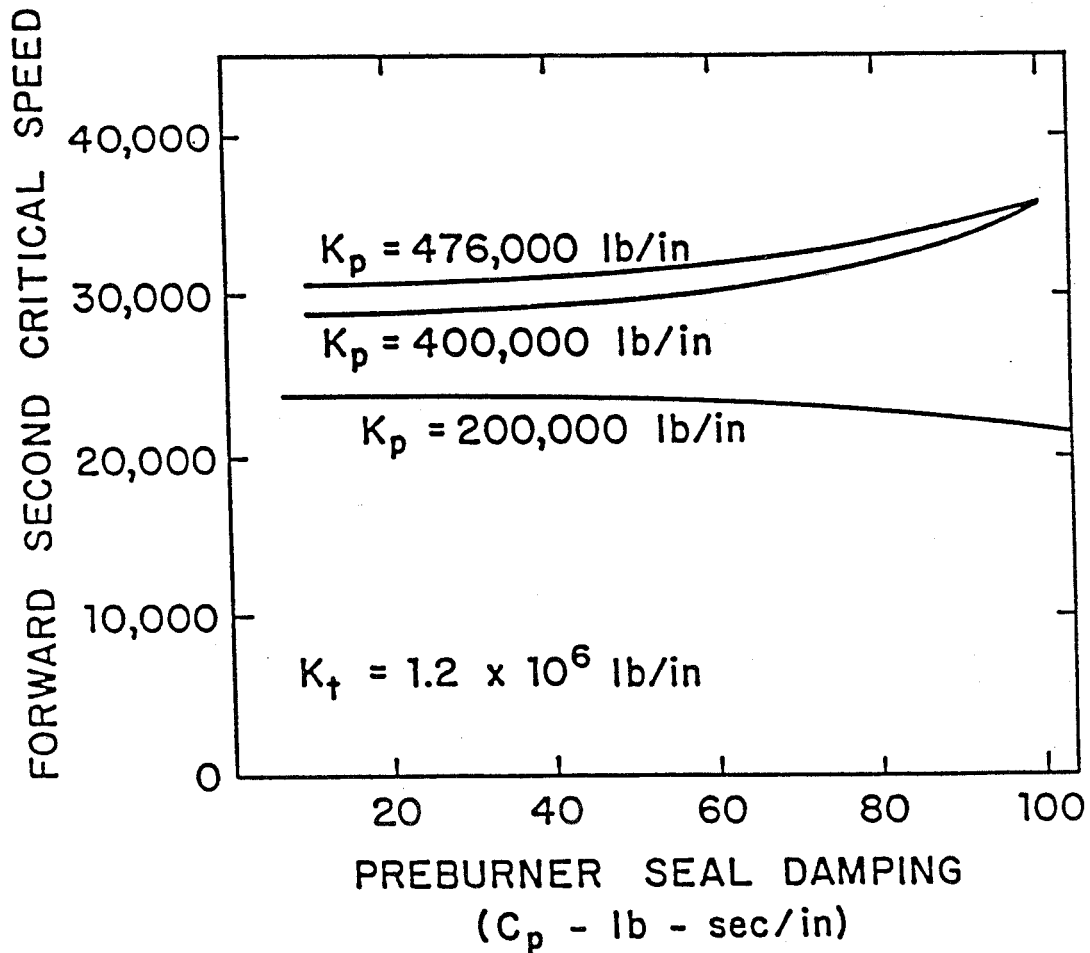## FOR VARIOUS LEVELS OF K_p & C_p

FIGURE 23

Analysis of the stiffened rotor was also performed in a manner similar to that presented in Figure 20. In Figure 24, the stability of the second mode is plotted as a function of the turbine bearing stiffness and of the preburner seal damping. The stability of the first mode is also indicated by the use of solid and dashed lines. A pump bearing stiffness of 200,000 lb/in was selected and the use of a stiffer pump bearing, as discussed previously, would require the inclusion of some additional damping, as indicated by Figure 22. The damping exponent indicates that the use of a stiffened rotor alone will stabilize the second mode. Thus, the selection of bearings and seals for the new rotor cross-section should be based on obtaining a stable first mode and an acceptable second critical speed.

DAMPED SECOND MODE
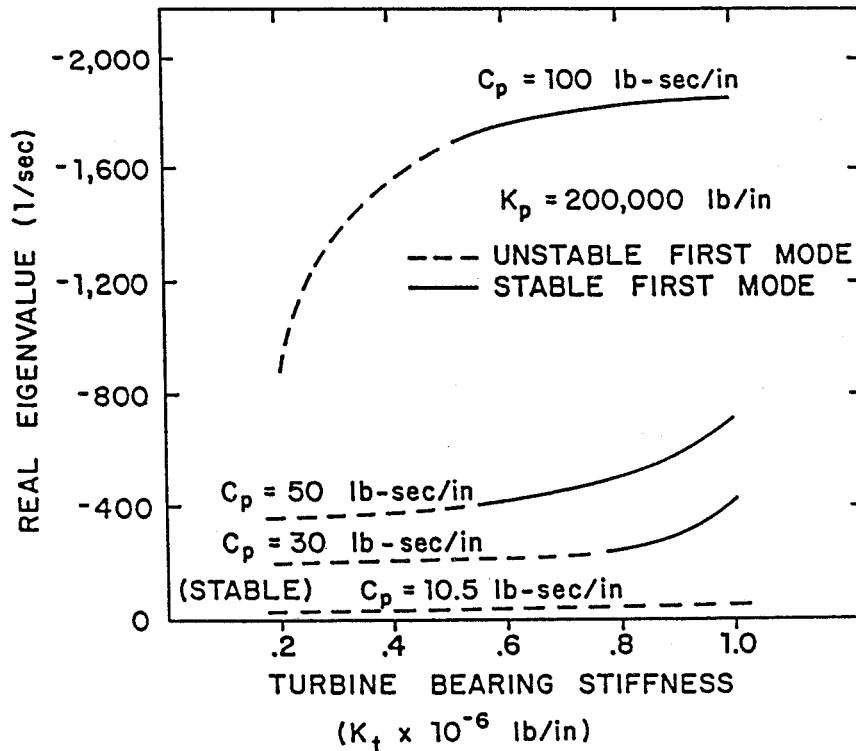## FOR VARIOUS LEVELS OF PREBURNER DAMPING
— STIFFENED ROTOR —

FIGURE 24

CONCLUSIONS

The experimental data available from the test operations of the liquid oxygen pump for the SSME repeatedly show the presence of resonant frequencies within the operating range of the pump. Critical speed analysis indicates that the presence of the second critical frequency is due to the pump and turbine bearings having stiffness values approximately 50% of the original specifications.

In modeling the pump rotor for computer analysis, discrepancies were found between the cross-sections of the NASA model (as derived from the inertia values) and the actual rotor cross-sections. The NASA model has a stiffer turbine section than is warranted. An alternate model (UVA) was developed from the actual rotor cross-section in order to provide a more suitable foundation for the stability analysis. Correlation between experimental balance data and the two rotor models supports the use of the UVA configuration. Little difference exist between the models when considering the second mode; both models predict the second critical speed to be within the operating range of the pump.

The oxygen pump rotor shows two bending modes of interest. The first occurs at 13,000 RPM and is primarily an overhung turbine mode. Due to interstage seal cross-coupling, this mode is linearly unstable. The second mode occurs at 27,000 RPM and is a main impeller-preburner mode. This mode is predicted to be unstable as a result of aerodynamic forces acting on the main impeller, for values in excess of 10,500 lb/in. Thus, both the first and second modes exhibit instability in the linearized system.

The instability of the first two modes, as well as the presence of the second critical frequency within the operating range, indicates modifications of the original oxygen pump rotor may be necessary. Simple adjustment of the bearings and seals will not provide sufficient support and damping

341

to insure stability: a stiffer shaft is required, primarily at the preburner pump bearing location.

The stability analysis supports the following conclusions:

1) The application of damping at the preburner seal location (by means of a full seal) will slightly improve the stability of the first mode, for damping values as high as 200 lb-sec/in, with the original rotor design.

2) Stiffening the rotor through the pump bearing section increases the effectiveness of the damping acting at the preburner seal location.

3) A large increase in the first mode damping is achieved with the stiffened rotor by reducing pump bearing stiffness from 476,000 to 200,000 lb/in.

4) Reduction of turbine bearing stiffness causes a loss in damping for the first mode, indicating that turbine bearing dead bands should be minimized.

5) For a stiffened rotor and turbine bearing stiffness of 1.2E6 lb/in, a reduced pump bearing stiffness will drop the second critical speed to 24,000 RPM. For preburner seal damping of 40 lb-sec/in, the second mode will be well damped and much less sensitive to rotor unbalance.

6) The stability of the second mode of the stiffened rotor is unaffected by aerodynamic cross-coupling at the main impeller, for values up to 40,000 lb/in. Figure 24, however, shows that the first mode may be unstable if the turbine bearing stiffness falls below 500,000 lb/in.

The stiffened shaft will stabilize the second mode. The addition of stiffer turbine bearings and a full preburner seal should then stabilize the first mode, as well as attenuate the second mode so that it will be insensitive to unbalance.

The following recommendations are made:

1) The original oxygen pump is unsatisfactory from a dynamics standpoint.

2) Modification and suitable redesign of a stiffened oxygen pump rotor and casing is desirable.

3) A full seal should be incorporated at the preburner seal location to increase damping for both the first and second modes.

4) The turbine bearing stiffness should be maintained as high as possible.

5) The use of dead bands in the turbine bearing should be minimized or avoided.

REFERENCES

1. Alford, J. S., 1965, "Protecting Turbomachinery from Self-Excited Whirl," ASME **Journal of Engineering for Power**, pp. 333-334.

2. Allaire, P. E., Gunter, E.J., Lee, C. P., and Barrett, L. E., "Final Report -- The Dynamic Analysis of the Space Shuttle Main Engine-High Pressure Fuel Turbopump, Part II, Load Capacity and Hybrid Coefficients for Turbulent Interstage Seals, Report No. UVA/528140/ME76/103 (September 1976).

3. Allaire, P. E., Lee, C. P., and Gunter, E. J., "Dynamic Analysis of SSME Plain and Plain Stepped Turbulent Seals," Report No. UVA/528140/MAE78/110, September 1978.

4. Black, H. F., 1969, "Effects of Hydraulic Forces in Annular Pressure Seals on the Vibrations of Centrifugal Pump Rotors," *Journal of Mechanical Engineering Science*, 11(2), pp. 206-213.

5. Childs, D. W., "Finite-Length Solutions for Rotor-dynamic Coefficients of Turbulent Annular Seals," *Journal of Lubrication Technology*, Vol. 105, pp. 437-444.

6. Childs, D. W. and Williams, J. P., 1989, "Influence of Impeller Shroud Forces on Turbopump Rotor Dynamics," ASME DE-VOL, 18-1, *Rotating Machinery Dynamics*, pp. 41-49.

7. Childs, D. W., 1978, "The Space Shuttle Main Engine Pressure Turbopump Rotor Dynamic Instability Problem," *ASME Journal of Engineering for Power*, Vol. 100, Jan., pp. 48-57.

8. Ek, M. C., 1980, "Solving Subsynchronous Whirl in High-Pressure Hydrogen Turbomachinery of the SSME." *J. Spacecraft*, Vol 17, No. 3, pp. 208-218.

9. Flack, R. D., Gunter, E. J., and Heinzman, J. D., "Experimental Data Analysis of the Space Shuttle Main Engine -- High Pressure Fuel and Oxidizer Turbopump," Report No. UVA/528140/MAE78/106, June 1978.

10. Gunter, E.J., 1966, "Dynamic Stability of Rotor-bearing Systems," NASA CP-113, Washington.

11. Gunter, E. J., and Flack, R. D., "Experimental Measurements of the Space Shuttle Main Engine Fuel and Oxygen Turbopump Vibration Characteristics," *Proceedings of the 27th International Instrumentation Symposium*, Indianapolis, Indiana, Instrumentation in the Aerospace Industry - Advances in Test Measurement, Vol. 18, Part 2, pp. 393-397 (April 1981).

12. Gunter, E. J., Barrett, L. E., Palazzolo, A. B., and Allaire, P. E., "Final Report -- Dynamic Analysis of the Space Shuttle Main Engine - High Pressure Fuel Turbopump, Part III, Linearized Stability Analysis," Report No. UVA/528140/ME76/104 (September 1976).

13. Gunter, E. J., Choy, K. C., Allaire, P. E., and Barrett, L. E., "Final Report - - The Dynamic Analysis of the Space Shuttle Main Engine - High Pressure Fuel Turbopump, Part IV, Unbalance Response Analysis," Report No. UVA/528140ME76/105 (September 1976).

14. Heinzman, J. D. and Gunter, E. J., "Experimental Data Analysis of Subsynchronous Excitation of the Space Shuttle Main Engine High Pressure Oxidizer Turbopump," Report No. UVA/528140/MAE78/112, September 1978.

15. Li, D. F. and Gunter, E. J., "Linear Stability Analysis of Dual Rotor Systems -- A Manual for Use with the Computer Program STAB2V2," Report No. UVA/464761/MAE79/154, September 1978.

16. Li, D. F. and Gunter, E. J., "Space Shuttle Main Engine High Pressure Oxidizer Turbopump Critical Speed and Unbalance Response Analysis," Report No. UVA/528140/MAE78/116, October 1978.